Ageing Effects of a Hall Thruster Plume on Solar Array Performance and ESD Susceptibility

IEPC-2017-493

Presented at the 35th International Electric Propulsion Conference
Georgia Institute of Technology • Atlanta, Georgia • USA
October 8 – 12, 2017

Jason A. Young[1] and Mark W. Crofton[2]
The Aerospace Corporation, El Segundo, CA, 90245, USA

Michael Glogowski[3] and Mike Eskenazi[4]
Orbital ATK, Dulles, VA, Zip Code, USA

Abstract: A test campaign has been conducted at The Aerospace Corporation under contract to Orbital ATK to assess the impact of a Hall thruster plasma plume on the functional performance and electrostatic discharge (ESD) susceptibility of a solar array coupon. The coupon was subjected to a mission life-equivalent ion exposure with a flight-representative XR5 Hall thruster. ESD tests were performed on the coupon before and after exposure to the plasma plume and were designed to assess the array characteristics under inverted gradient and normal gradient charging conditions. In addition, the combined effect of Hall thruster startup on an environmentally charged coupon was examined. Functional testing was performed on the coupon before and after thruster ageing and including electro-luminescence and Large Area Pulsed Solar Simulation (LAPSS) testing. The key findings of this study are presented here.

Nomenclature

C_{str}	=	structure capacitance
C_{stg}	=	series capacitance of missing cells for string 2
C_{sub}	=	parallel capacitance to substrate of missing cells for string 2
I_{sc}	=	short circuit current of a cell or string
I_{load}	=	current of a cell or string under nominal load
$R_{1,2}$	=	test circuit resistance parallel to string 1,2
R_{stg}	=	test circuit resistance in series with string 2
$V_{1,2}$	=	nominal voltage across string 1,2
V_{bus}	=	bus voltage
V_{clamp}	=	clamping voltage
V_d	=	voltage drop across protection diode
V_{oc}	=	open circuit voltage of cell
V_{stg}	=	voltage across drop string on full panel, less the voltage drop across string 2
P_{max}	=	max power of cell

[1] Member of Technical Staff, Propulsion Science Dept, Jason.A.Young@aero.org.
[2] Senior Scientist, Propulsion Science Dept, Mark.W.Crofton@aero.org.
[3] Senior Director, Adv. Tech. Dev., Satellite Systems Division, Michael.Glogowski@OrbitalATK.com.
[4] Chief Engineer, Space Components Division, mike.eskenazi@orbitalatk.com.

I. Introduction

THE plasma plume produced by an ion electric propulsion system introduces new environmental conditions, for which spacecraft engineers must design and develop systems that can operate reliably over the required mission lifetime. This environment is analogous to the low earth orbit environment in terms of the plasma number densities but is different in that the plasma plume species travel at sufficiently high velocity to cause sputtering of any spacecraft surface that comes within its path. This sputtering will in turn result in re-deposition and contamination of other spacecraft surfaces that are within the line of site of the re-emitted material. Other effects produced by this plasma environment include parasitic currents through the spacecraft power system, which could magnify the sputtering and re-deposition process and possibly lead to reductions in solar array efficiency for high voltage arrays. The plasma environment could also interfere with the propagation of radio-frequency waves, such as those produced by the spacecraft Telemetry, Tracking and Command (TT&C) subsystem and the main communications system of commercial geostationary satellites.

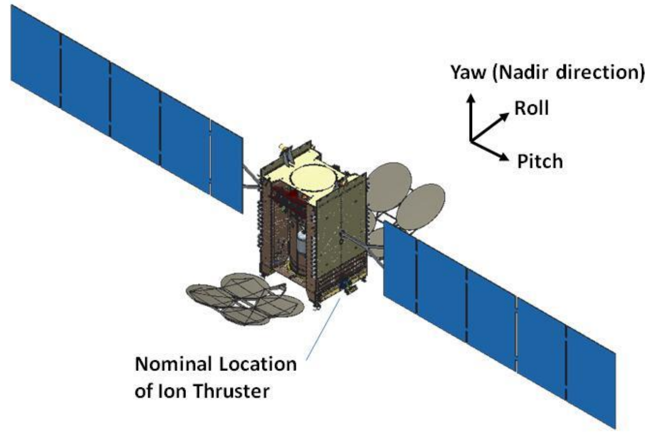

Figure 1. Notional Geostationary Satellite with Ion Electric Propulsion.

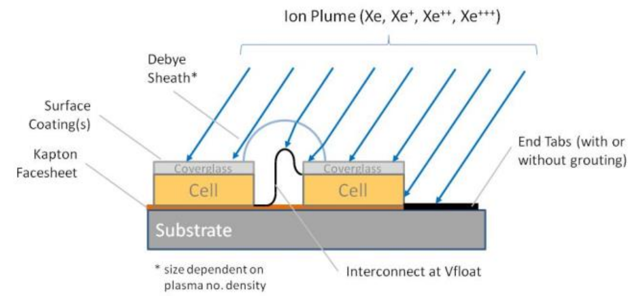

Figure 2. EP Plume Interactions with Solar Cell & Interconnect.
Electric propulsion devices produce high energy ions that can erode surfaces and plasmas that can electrically couple to exposed conductors and rapidly neutralize surface charge

This situation exists for the two common forms of ion electric propulsion (EP) systems, namely the Hall thruster and gridded ion thruster. The differences lie only in the distribution of the plume's ion energy and current and the physical material that is emitted from the thruster due to self-erosion. For the Hall thruster, on which this paper is focused, the plasma plume consists of multitude of species, including high energy ions at different charge states, high energy neutrals and low energy ions that form through a charge exchange process between a high energy ion and xenon neutral, free electrons, and physical material sputtered from the thruster itself. This material could include the insulator material that surrounds the plasma discharge and isolates it from the magnetic poles or the magnetic pole material itself if the insulating material has been eroded away by the thruster. Unlike conventional chemical plumes but common with the gridded ion thruster, the Hall thruster plume will follow electric field lines and extend out to very wide angles, including angles greater than 90˚ from the thruster center line. As a result, it is impossible to isolate the spacecraft, solar array and other appendages from the influences of the plasma plume.

Placement of the thruster on the spacecraft can greatly reduce these effects but not eliminate them entirely. For geostationary satellites, which are typically comprised of two solar array wings extending in opposite directions along the spacecraft pitch axis and one or more communications antennae extending along the spacecraft roll axis, the ion electric thrusters are placed at the aft end of the spacecraft close to the spacecraft centerline as shown in Figure 1. At this location the thruster plume is nominally behind the communications payload and pointed away from the solar array wing with a modest cant angle. For optimal propellant efficiency the thruster should be pointed in the same direction as the solar array, except that it puts the array in the high density and high energy region of the ion electric thruster plume. As a compromise between maneuver efficiency and solar array compatibility, the thrusters are oriented with this cant angle to minimize the erosive effects of the electric thruster plume. In some applications the thrusters are deployed away from the spacecraft on a boom to further reduce the plasma plume effects at the expense of increased mechanical system complexity. However, the effects will still occur, but only at a reduced magnitude.

Verification of spacecraft compatibility to this environment is a complex process, typically involving high fidelity models anchored against experimental data [1]. While no standard has been established, the process is viewed by prime contractors and customers alike as sufficient for evaluating the global effects of plume sputtering and re-deposition as well as RF propagation effects. These global effects include, but are not limited to, reduction in solar cell efficiency through a loss in cover glass transmissivity, an increase in thermal radiator absorptance through deposition of a contaminant layer from material sputtered from the solar array [2], and beam pointing errors due to phase delay of RF signals propagating through the plume [3].

However, this approach cannot address adequately the higher order effects and complex geometries associated with the active side of the solar array as shown in Figure 2. For example, sputtering of the end tabs or exposed interconnects could lead to cross-contamination of the cell as observed in Reference [4]. Etching of the cells in a preferential manner may affect light transmission at perpendicular [5] or non-perpendicular incidence angles, which occur during solstice seasons on geostationary communications satellites. And, most importantly, the erosion of the cover-glass, interconnects, grouting and face sheet could fundamentally modify the onset, frequency and magnitude of electrostatic discharges under inverted gradient or normal gradient conditions. Furthermore, the array under these electrostatic discharge (ESD) susceptible conditions may behave in an unforeseen manner when the plasma plume is first initiated, contrary to the expectation that the plasma plume provides a dissipative environment for these high voltage conditions.

For the purpose of verifying solar array design compatibility to this environment, a test campaign was conducted at The Aerospace Corporation under contract to Orbital ATK whereby a solar array test coupon was exposed to the plasma plume of the XR-5 Hall thruster under conditions that achieved a total ion flux exposure equivalent to a full mission life at an incidence angle and ion energy distribution representative of worst-case flight conditions. This ageing test was preceded and followed by a series of electrical, ESD and performance tests to characterize the changes in these parameters. It also included an assessment of the plasma initiation effects on highly charged surfaces and of the steady-state plasma environment on ESD breakdown conditions. Results of this test campaign are reported here.

II. Experiment Description

A. Solar Array Coupon

The goal of this test campaign was to investigate the effect of various natural and artificial plasma environments on spacecraft solar arrays. To achieve this end, a reduced scale (22.9 cm x 40.6 cm) solar array coupon was created, which incorporated essential characteristics of a full solar array panel. As shown in Figure 3, the Solar Array Test Coupon (SA Test Coupon) was comprised of nine XTJ Coverglass-Interconnected-Cells (CICs), electrically connected to form two solar cell strings (one with 3 cells, and the other with 6 in a serpentine arrangement).

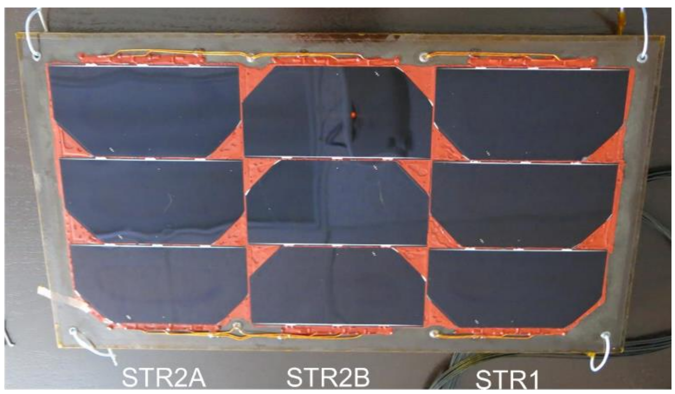

Figure 3. Solar Array Test Coupon.
String 2 is composed of the left two columns of cells, connected in a serpentine series, with the positive terminal on the top of the center substring. String 1 is the last column of cells, with the positive terminal on the bottom.

B. Test Sequence

The overall test sequence is enumerated in Table 1. At the beginning and end of the campaign, a complete series of ex-situ functional tests were performed, described below. In the middle of the test campaign, the coupon was subjected to an accelerated thruster ion beam exposure simulating lifetime exposure. Tests before this exposure are designated as beginning of life (BOL), and after as end of life (EOL). The remaining tests consisted of a different representative space charging environments. The values for STR1-, STR1+, STR2-, and STR2+, refer to the applied biases at each terminal of each string during the test. In between each test, limited in situ functional tests were performed. Details are discussed below.

C. Functional Tests

Before and after exposure to a series of plasma environments at the Aerospace Corporation, a complete series of functional tests were performed on the test article. These included forward and reverse biased dark IV tests (bypass diode and cells), insulation resistance checks, electroluminescence (EL) and Large Area Pulsed Solar Simulation (LAPSS) testing. LAPSS testing was conducted at normal incidence angle as well as off-axis for evaluation of the effect of the observed plasma etching on light collection efficiency.

Table 1. Coupon Exposure Test Sequence.

Test Condition	***Electron Gun***	***Coupon Bias***	***Str1+***	***Str1+***	***Str2+***	***Str2-***	***Thruster***
BOL Full Functional Tests	--	--	--	--	--	--	--
BOL Inverted Gradient	5 keV, 1nA/cm^2	-4 kV	0.4 V	0.0 V	39.5 V	29.2 V	None
BOL Normal Gradient	20 keV, 1nA/cm^2	0 kV	0.4 V	0.0 V	39.5 V	29.2 V	None
BOL Inverted Gradient with EP Startup	5 keV, 1nA/cm^2	-4 kV	0.4 V	0.0 V	39.5 V	29.2 V	1kW Lab
BOL Normal Gradient with EP Startup	20 keV, 1nA/cm^2	0 kV	0.4 V	0.0 V	39.5 V	29.2 V	1kW Lab
Accelerated Lifetime EP Ion Exposure	--	--	0.0 V	0.0 V	0	0	XR5
EOL Inverted Gradient	5 keV, 1nA/cm^2	-4 kV	0.4 V	0.0 V	39.5 V	29.2 V	None
EOL Normal Gradient	20 keV, 1nA/cm^2	0 kV	0.4 V	0.0 V	39.5 V	29.2 V	None
EOL Normal Gradient with EP Startup	20 keV, 1nA/cm^2	0 kV	0.4 V	0.0 V	39.5 V	29.2 V	1kW Lab
EOL Inverted Gradient with EP Startup	5 keV, 1nA/cm^2	-4 kV	0.4 V	0.0 V	39.5 V	29.2 V	1kW Lab
EOL Full Functional Tests	--	--	--	--	--	--	--

In order to monitor changes in string health between ESD and EP test conditions, in-situ measurements of string dark IV curves were performed. Due to limitations of the vacuum feedthrough, a simple 2-wire setup was used for each substring of 3 cells, resulting in somewhat reduced fidelity due to spurious voltage drops along the long harness. The blocking diodes on the back of the coupon were bypassed so both forward and reverse bias could be measured. To improve repeatability, the string temperature was maintained near ambient by heater lamps behind the coupon. In situ EL measurements were also performed between test conditions. These consisted of applying a bias across the substring and taking a photograph with a color camera. If new dark or bright spots appeared after a given test condition, this was taken as evidence of cell alteration.

D. XR-5 Lifetime Ion Exposure Setup

Coupon ESD and EP exposures took place in EP2, an 8' diameter vacuum chamber with a nominal pumping speed of 250kL/s for Xenon. A schematic of the setup for the lifetime thruster plume exposure is shown in Figure 4. The goal here was to accurately simulate worst-case sputter erosion of a thruster ion plume on an accelerated timetable rather than simulate plasma flux or density at one-to-one scale. A 3 kW XR-5 Hall thruster was used, running at full power, to provide a high fidelity reproduction of ion energy distribution impinging on the solar panel. The geometry was adjusted to reasonably simulate worst-case plume impingement on a solar array. The long dimension of the coupon was oriented upward so that the string pointed toward or away from the thruster. To achieve maximal sputter yield, the coupon was canted such that the angle of incidence of the thruster ions on the coupon was 60°. The distance was reduced to 0.9 m to significantly accelerate lifetime exposure.

A conventional unguarded planar probe beneath the coupon (but at the same 55° plume angle) was used to verify total ion exposure. The coupon itself was mounted off of a plate heated by a Kapton heater. This ensured it was possible to continue performing in-situ dark IV and EL tests in between exposures (without the heater, the coupon would be cooled to -29°C, significantly shifting the dark IV curves). To protect the coupon from sputtered carbon coming off the opposite wall of the chamber, a Grafoil-covered sputter shield plate was installed in front of the coupon. The shield was placed as close as possible to the coupon without obstructing the thruster plume. It was canted such that the thruster plume had no field of view to coupon-facing side and grazing incidence on the opposite side. The grafoil shield extended all the way to the wall near the coupon to protect it from backscattered carbon as well.

E. ESD Charging Setup

The internal setup for electron beam and combined electron beam and Hall thruster plasma exposure is shown in Figure 4. The coupon was mounted off an aluminum plate on the wall of the chamber, with Delrin posts for electrical isolation. A Kimball Physics electron flood gun on the opposite wall of the chamber irradiated the coupon with electrons at normal incidence. The coupon was surrounded by four compact Faraday cups with 1 cm^2 collection area. The current on the cups was used to fine tune the electron gun rastering and ensure a uniform flux of 1nA/cm^2 on the coupon. A Trek contactless electrostatic probe mounted off an arm on a two axis stage allowed for surface potential measurements on the coupon following irradiation. A calibration plate mounted adjacent to the coupon was used to correct the zero offset of the Trek probe. A Vision Research Phantom Miro4 high speed color camera, mounted outside a window on the chamber, was used to capture images of ESD events on the coupon.

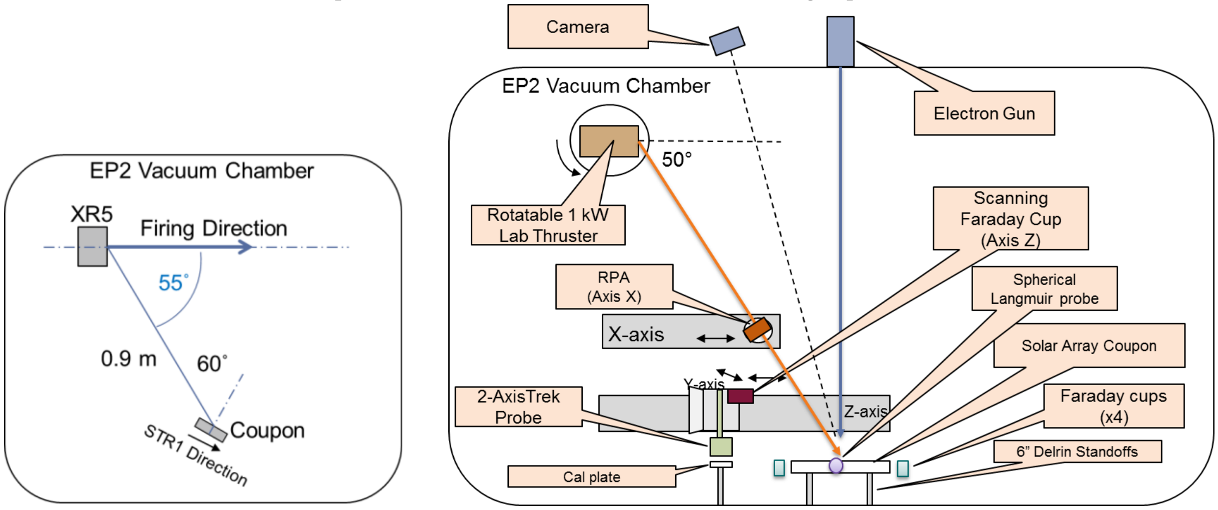

Figure 4. Coupon Exposure Setups. *A simplified top view of the XR5 accelerated lifetime exposure geometry is shown on left. A top view of the combined electron beam and thruster plume exposure setup is shown on right.*

For normal gradient (NG) tests, the electron gun was run at 20 keV. This simulated the eclipse condition on a solar array and resulted in a net negative surface charging on the coupon surface. The 1nA/cm^2 current density was chosen to provide a typical worst case GEO test environment. For inverted gradient (IG) tests, the electron was run at 5keV and the coupon was biased 4kV, resulting in significant secondary emission of electrons from the coupon surface. In this way, a net positive surface charge could develop, similar to a sunlit condition.

F. Combined ESD & EP Plasma Setup

For combined effects tests, the coupon was exposed to the plume of a 1kW lab thruster shortly after exposure to normal or inverted gradient electron beam conditions. Further details about this thruster are discussed in past literature [6,7]. The goal of this test was to simulate plasma interactions with a charged solar panel following startup of an on-board electric propulsion device. As such, the distance and angles between the coupon and thruster were adjusted to provide an ion flux, energy distribution, and ion density (in that order) similar to what might be experienced by a solar panel on-orbit. As shown in Figure 4, the thruster was on a rotatable stage 2 m from the coupon, 50° off the centerline of the thruster plume (~40° angle of incidence on the coupon). Because the on-orbit distances between the thruster and panel are significantly larger than the dimensions of the chamber, the thruster was run at reduced power (1A, 400V). The ion flux at the coupon was approximately 1.4 μA/cm^2 and the density was on the order of 10^{13} m^{-3}. A

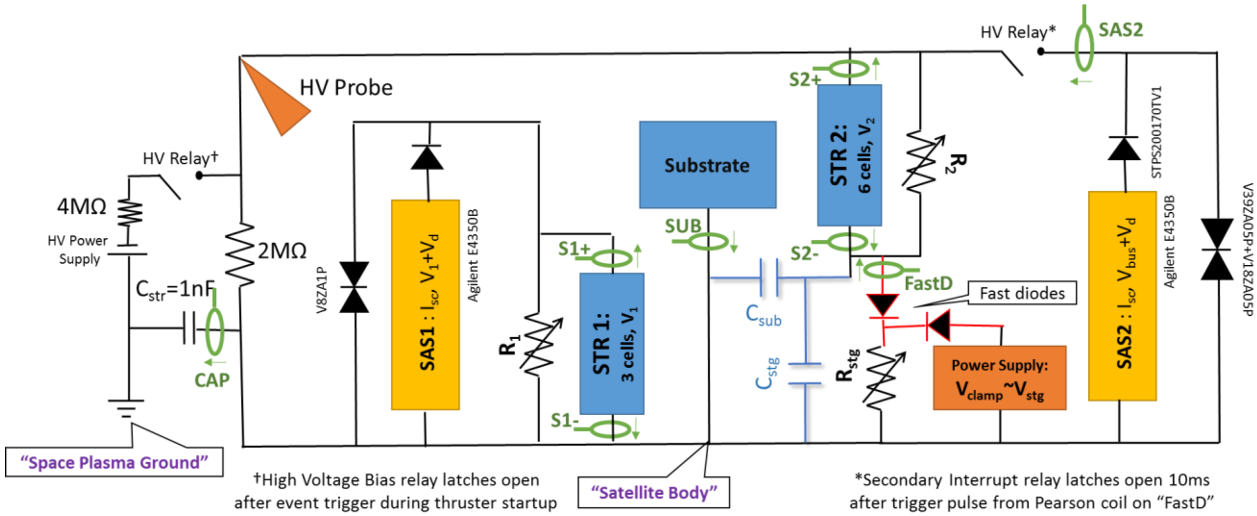

Figure 5. ESD Test Circuit. *Coupon strings were attached to this external circuit during ESD testing.*

retarding potential analyzer (RPA), swept along the edge of the plume at normal incidence, was used to verify the desired ion energy distribution was achieved.

Designing a system that was interoperable in both a high energy electron environment and a low density plasma environment was not entirely trivial. Insulator surfaces had to be protected from high energy electrons to prevent spurious ESD events. Another example was the Langmuir probe used to characterize plasma conditions from the 1kW thruster plume. Typically, a normal incidence planar Langmuir probe would be used to measure flux and plasma density from a Hall thruster plume. However, the conventional planar probe has many exposed insulators and would be prone to electrostatic arcing in a high energy electron beam. Instead, a 1.27cm diameter spherical Langmuir probe, mounted above the coupon, was used to verify (approximately) the plasma conditions in the vicinity of the coupon. The ion saturation current of the probe at negative bias could then be used to determine ion flux, assuming a normal area of 1.27 cm^2. Ion density could then be derived by dividing out the average ion velocity, which can be determined from the RPA energy distribution.

G. ESD Test Circuit

Considerable thought went into the design of the external circuit for ESD testing. The goal was to determine whether a primary electrostatic discharge could trigger a secondary arc between adjacent strings if one string was powered. On the full panel being simulated, the voltage drop across a fully powered 23-cell string is regulated to V_{bus}=39.5V. This voltage drop is a natural consequence of illuminating the photovoltaic cells. In this case I_{load}=1.23A flows from the negative terminal of the cell to the positive terminal, like a battery. Ideally, one would try to perfectly recreate this condition in the laboratory. However, illuminating an entire coupon with 1 sun equivalent of intensity through a vacuum port window 2.5 m away was beyond the technical scope of this campaign. Instead, we applied voltage bias to the strings via an external circuit, with a circuit design inspired by past literature, including the ISO standard for secondary arc testing of a solar array coupon [8-10].

A consequence of not illuminating the strings is that to achieve a bias, one must flow current through the cells from the positive terminal to the negative terminal, in the opposite direction to the illuminated case. Since the dark cell acts like a conventional diode, current grows exponentially with bias voltage. If the voltage bias is set to the on-orbit operating voltage, the unilluminated current is orders of magnitude lower than the illuminated current. The full on-orbit current can only be achieved close to the illuminated open circuit voltage. Since it is impossible to achieve both the illuminated current and voltage simultaneously on a dark string, we opted for voltage, in keeping with the ISO standard and other studies [8-10].

The ESD circuit used in this test campaign is shown in Figure 5. It was designed to simulate a full string at nominal voltage (serpentine STR2) placed anti-parallel with a shunted string (STR1). Hence, string 2 had a voltage drop across its cells and was biased relative to the string 1, which had negligible voltage drop across its cells. During steady state operation, voltage biases across and between strings were provided by Agilent E4350B Solar Array Simulator (SAS) power supplies. These low-capacitance supplies were run in constant current mode (solar array simulation does not have a sufficiently rapid response time, resulting in higher effective capacitance than constant current mode) with a voltage limit set at the worst-case open circuit voltage for a full string. Similar to the Huntsville group design, high power resistors and potentiometers in parallel and series with the SAS supplies (R_1, R_2, and R_{stg}) set the appropriate voltage drops, since little current can flow through the cells themselves [8]. A capacitor C_{sub}=13nF was added between STR2 and substrate to simulate the missing cells from a full string [8-10]. The series capacitance of missing cells C_{stg} was assumed to be negligible. In order to protect the SAS units during ESD events, a transient voltage suppressor was inserted in parallel and a diode was inserted in series to block back-flowing current. SAS voltages were increased accordingly to correct for the drop V_d across these protection elements. Before pumping down the chamber, the SAS supplies were energized and voltage differences are verified directly on the coupon with a handheld multimeter.

In terms of the relationship of this string powering scheme to on-orbit conditions, the most obvious case is for inverted gradient, where power bus throttling can result in one illuminated string at full voltage next to another at minimal voltage. The normal gradient case is a bit rarer. It corresponds to the condition exiting eclipse or shadowing, where the panels are still at high negative voltage but are beginning to be illuminated. The modest voltages on the cells should have little effect on the high voltage primary discharges so for the purposes of determining primary discharge statistics, this is similar to a more conventional unpowered normal gradient test. For secondary discharges, due to the rarity of the condition being tested, it is likely these exposures exceeded normal lifetime exposures.

The entire ESD circuit, including the SAS power supplies and clamping power supply, was electrically floated using a 10kV-rated transformer. A 1 nF structure capacitor between the circuit and ground was inserted to represent the finite capacitance to space. An SRS PS350 high voltage supply with a 4MΩ isolation resistor allowed the entire circuit to be biased to -4 kV during inverted gradient charging. For normal gradient testing, the power supply was bypassed but the 4MΩ resistor remained so the circuit still floated during discharge events, similar to the setup of Leung [11].

SAS currents and voltages and clamping voltages were monitored continuously via a fiber optic GPIB connection to a data logging computer. Current and voltage signals from on this external circuit due to primary discharge were monitored by two Tektronix scopes triggered by a primary discharge current flowing into the structure capacitor (threshold and slope adjusted for normal versus inverted gradient conditions). Automated Labview software captured each event and synchronized the trigger arming of each scope. The trigger signal for the scopes also triggered high speed camera capture.

Tektronix TCP202, TCP303, and TCP0020 current probes, represented by green ovals in Figure 5, monitored current going in and out of each string terminal, current flowing from the coupon substrate to common, current flowing into the structure capacitor, and current flowing into fast diode. A Lecroy 20kV scope probe monitored the overall voltage of the floating external circuit during discharge. When high voltage bias was applied to the circuit, a small, 50 Vpp ripple appeared in the high voltage signal due to cross coupling between the AC power inputs and DC outputs of the SAS supplies, by way of their floating chasses (which would usually be grounded for typical applications). This was deemed largely unavoidable as the alternatives involved directly or indirectly adding non-flight-like capacitance or reducing the isolation resistance.

A few modifications had to be made to the ESD test circuit during combined electron beam and thruster exposure conditions. Current probes monitoring cathode and anode currents of the thruster during startup were added to the long time base oscilloscope. As will be discussed in the results section, a variety of different triggering schemes were attempted to better capture transient events. The time base and resolution of all the scopes were increased to capture the entire thruster startup. The high speed camera was set to capture continuously for a few seconds, instead of capturing a single frame at the time of the primary discharge.

The high voltage bias supply used in inverted gradient combined effects tests was particularly problematic. If left running during startup, it would cause repeated, non-flight-like snap-over of the solar array coupon. To correct this, a shutoff circuit was employed, similar to the secondary discharge interrupt discussed in the next section. In this case, a high voltage relay interrupted the current from the HV bias supply immediately after a scope trigger. In addition, the bias supply voltage was manually reduced to -1kV, immediately after electron gun shut down and before thruster startup. This -1kV bias was sometimes also used for normal gradient combined effects tests as it made it easy to detect activity on the external circuit.

H. Secondary Discharge Sub-circuit

In a real solar array secondary discharge, photovoltaic current would flow up from common to the negative terminal of a cell on string 2, then cross through the arc to a cell at lower voltage on string 1. The plasma short between two arcing cell would cause the voltage across the substring below the arc point on string 2 to slump. However, because the cells are still illuminated, it would not reduce their ability to source at least as much current as they provided before the arc. The substring above the arc would then respond as if the lower substring were completely shadowed. With a fixed bus voltage and a blocking diode that prevents backflow of current, this would result in the upper substring cells getting pegged at their respective open circuit voltages. If there were multiple strings per blocking diode, additional current might flow up from the adjacent string and in reverse down string 2 until their voltages are in equilibrium.

Similar to various previous studies [8-10], a clamping voltage circuit was added to the ESD circuit shown in Figure 5 to better replicate some aspects of the effect described above. The clamp voltage is set slightly below the voltage drop across the 24Ω bias resistor so that clamp supply current flowing through the fast diode to the bias resistor is negligible. During a secondary discharge, SAS2 current flows through string 2 to string 1 or substrate and the voltage on the negative terminal of string 2 slumps below the clamp voltage. In this case, the fast diodes shut off SAS2 current into the bias resistor and turn on clamp supply current into this resistor. In essence, the clamping voltage circuit quickly removes the bias resistor from the circuit during a discharge to ensure the full current of SAS2 can be delivered to the arc, similar to the full current delivered by the substring in a true arc.

Secondary discharge was detected by monitoring current going the fast diode downstream of string 2. If a secondary arc occurred, the current into the fast diode would drop. The length of the secondary discharge could then be estimated by the length of time that the fast diode current was at zero. A third Tektronix scope with longer time base monitored this current via a Tektronix current probe. In order to limit the damage in the event of a sustained discharge, a secondary interrupt circuit was included [8]. In essence, the fast diode current signal was used to trigger the opening of a high voltage relay between SAS2 and string 2 after 10ms. The relay would then latch open for a predefined period before resetting to the closed state. The time delays were produced by pulse time delay generators.

III. Results

The discharge statistics of the non-thruster ESD conditions are summarized in Table 2. Note that exposure times are determined based on statistical requirements (e.g. more than 50 captured events) and are not intended to be flight representative. Also note that the number of recorded events may be less than the total number actual event due to the limited capture throughput of the oscilloscope acquisition system. The transient current amplitudes and maximum voltages are given in absolute magnitude. The absolute value charge is derived by integrating the current signals.

A. BOL Inverted Gradient.

A total of 83 BOL inverted gradient discharges were recorded over a 2 hour exposure. A majority of arcs originated on the substrate, resulting in large positive current flow from the substrate to common, as measured on the external circuit. Surface potentials on the coupon rose as high as +1.9kV on the coverglasses and no more than a +1kV on the RTV (relative to the -4kV substrate bias, as measured by Trek probe). Figure 6a shows a typical substrate discharge current waveform and associated high speed camera image. Nearly 4A of electrons flow from the substrate to both the chamber wall and the positively charged coverglass surfaces. The portion that is emitted towards the wall, or "blow-off", relieves the 4µC structure charge stored in the circuit, resulting in 1.2A flowing into the capacitor. The remaining electron current, or "flashover", neutralizes coverglass surfaces, resulting in image currents of several tenths of amps returning into the cells.

As shown in Figure 6a, the arc center is indicated by a bright point in the lower right corner of the coupon. The flashover plasma interacts with the MgF_2-coated coverglasses to the left of the arc point, producing a pale blue glow.

Table 2. ESD Discharge Statistics for Non-Thruster Exposures.

Test Condition	*# of Recorded Events*	*Cumulative Exposure (hr)*	*Max |Surface Potential| (kV)*		*Substrate*				*String Terminal (S1+,S1-,S2+,S2-)*			
					|Current| (A)		*|Charge| (uC)*		*|Current| (A)*		*|Charge| (uC)*	
			Coverglass	*RTV*	*Max*	*Mean*	*Max*	*Mean*	*Max*	*Mean*	*Max*	*Mean*
BOL Inverted Gradient	83	2	1.9	1.0	4.08	1.76	19.6	12.1	2.36	0.44	28.8	4.1
BOL Normal Gradient	57	3	-8.0	<-10.5	60.2	28.6	58.6	24.1	25.2	6.3	30.7	5.8
EOL Inverted Gradient	100	0.65	1.2	1.0	0.33	0.44	3.7	1.85	1.72	0.51	22.7	5.7
EOL Normal Gradient	61	6.5	-13.5	-13.5	91.6	27.7	126	32.5	35.5	7.08	71	10.7

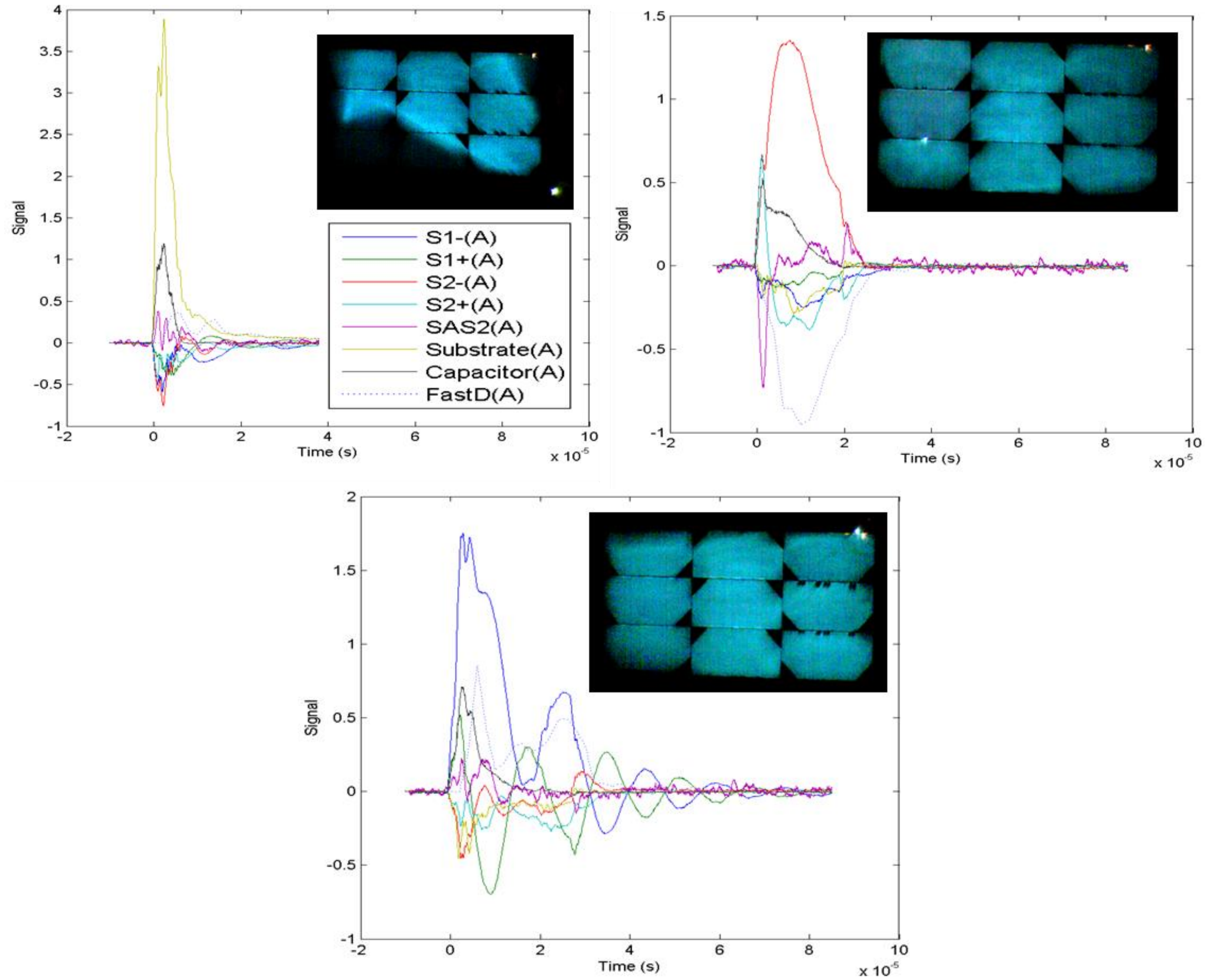

Figure 6. BOL Inverted Gradient Events. *Each plot shows current transients from an individual ESD event. Inset is the associated high speed camera image of that event. Top left (a) shows a substrate arc, top right (b) shows in interconnect arc, and bottom (c) shows a string termination arc.*

Unlike many published images of flashover glow, this one is highly asymmetric (see e.g. [11]). The raised prayer tabs in between cells on the right-most string appear to obstruct this plasma, resulting in dark shadows. The triangular grouted regions between cells are dark, suggesting that this flashover glow is likely a material-dependent cathodoluminescent effect (see e.g. [12]). Note the glowing orange point in the upper right corner is a reflection of the electron gun filament.

Figure 6b and c show examples of an arc at the cell interconnect and one at the string termination. In this case, the 4uC of blowoff and surface flashover current is being sourced by an individual string. These events are characterized by comparatively longer, lower amplitude positive current waveforms from a terminal of the affected string. In the case of the termination arc, a small oscillation occurs due to current flowing alternately from either end of string 1. Similar to the substrate discharges, the coverglasses are illuminated by a blue flashover glow, although in this case the distribution is more uniform. Figure 6c provides further evidence of shadowing of the flashover plasma by the prayer tabs on string 1.

There was no clear evidence of secondary arcing during any inverted gradient events. During a secondary discharge, the current flowing through the fast diode into the bias resistor should drop from 1.28A to 0A. Because of the orientation of the probe and baseline zeroing, this should manifest as a sustained 1.28A excursion. While many events showed nontrivial change in current across the fast diode and current between strings, this occurred only within the normal time envelope of the primary discharge. This transient current, which could sometimes exceed the nominal SAS current, was due to the rapid release of stored charge from various sources, including the SAS internal capacitance.

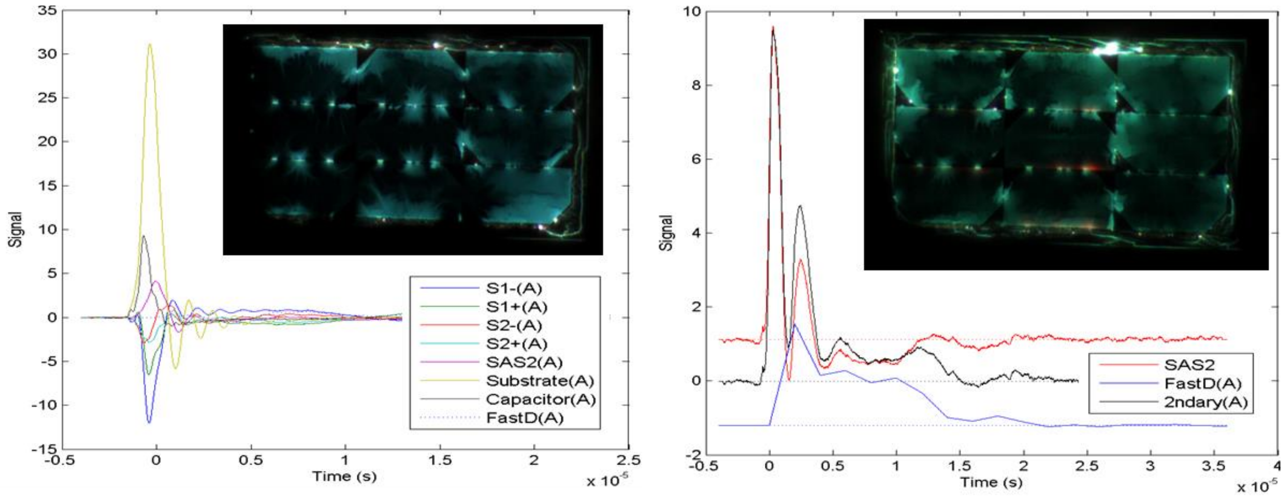

Figure 7. BOL Normal Gradient Events. *Each plot shows current transients in Amperes from an individual ESD event. Inset is the associated high speed camera image of that event. Left plot (a) shows a substrate arc, and right plot (b) shows a substrate arc that led to a secondary discharge. The latter plot indicates the current sourced from SAS2 into STR2+ in red, current flowing from the fast diode into STR2- in blue (should be -1.28A at steady state and 0A during discharge), and the net current flowing from STR2 into the secondary arc in black.*

B. BOL Normal Gradient

A total of 57 BOL normal gradient discharges were recorded over a 3 hour exposure. The overall statistics are given in Table 2. Surface charge on the coverglasses approached -8kV with RTV exceeding -10.5kV (the data acquisition signal was saturated). The arcs were dominated by the substrate contribution, with current transients up to 60A and 24µC. A typical discharge is shown in Figure 7a. The discharge duration was much shorter than for inverted gradient, only a few microseconds. Multiple bright arc points were seen along the perimeter of the coupon, with streamers tracing along wires. Coverglass luminescence was localized to the cell edges and interconnects.

For these test conditions, the principal mechanism for producing observable currents on the external circuit was blowoff of negative charges on from the surface of the coupon to the wall. The relative magnitude and direction of the currents was determined in part by the relative capacitances between cells, substrate, coverglass surfaces and exposed Kapton surfaces as well as the relative surface potentials on coverglasses versus bare Kapton. For this particular coupon, there was an excess of charge stored on the substrate, so when that charge was released via blowoff, voltage equilibrium was achieved by a net flow of positive current from the substrate to the cells via the external circuit common.

Another mechanism for charge flow is electron conduction into covered conductors via dielectric breakdown or directly into exposed conductors. Since this process neutralizes image charges directly at the coupon level, there are no return currents flowing through the external circuit. Strong evidence for this process can be seen from the high

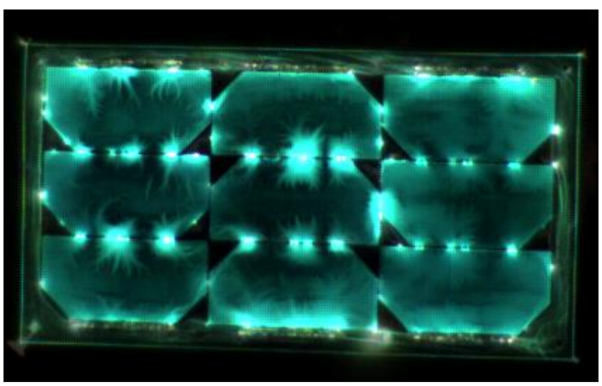

Figure 8. Composite Image of All BOL Normal Gradient Events. *This image shows a per-pixel average of all high speed camera frames taken during beginning of life normal gradient exposure.*

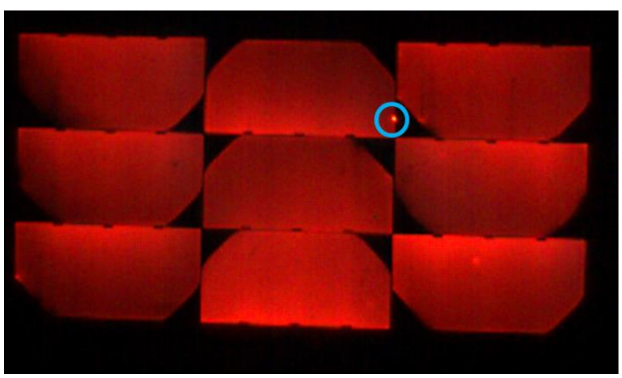

Figure 9. Electroluminescence After BOL Normal Gradient. *This image shows electroluminescence after BOL Normal Gradient exposure. A new hotspot feature is circled in light blue.*

speed imagery. Figure 8 shows a composite average of all discharge images taken at BOL Normal Gradient. In it, one can observe blue streamers emanating from the interconnects, terminations, and edges of the cells. Direct conduction of current through these streamers reduces the positive image current available to flow back from the strings to the external circuit. The arc points on the Kapton-covered substrate are themselves due to dielectric breakdown, which conducts a small fraction of the Kapton surface charge directly into the substrate.

During normal gradient testing, the coupon experienced a few temporarily sustained secondary arcs. An example of such an event is shown in Figure 7b. As shown in the high speed camera image, the primary arc occurred on the substrate between the negative terminal of string 1 and positive terminal of string 2. The FastD (fast diode) current drops to zero for 15us, well beyond the primary arc duration. This indicates the voltage clamping interrupt circuit is engaged and all SAS2 current is diverted into the arc. Meanwhile, the SAS2 current slumps to 0.5A after initially spiking up to 9A during the primary discharge (presumably due to capacitance stored in the SAS2 supply). The sum of FastD and SAS2 signals then indicates the total current flowing through the secondary arc is about 0.5A. Assuming the SAS2 supply is at its 61.5V voltage limit, this suggests a reduced impedance of ~120 Ohms between strings 1 and 2. This elevated voltage likely contributed to hint of electroluminescence observed at the interconnects of String 2.

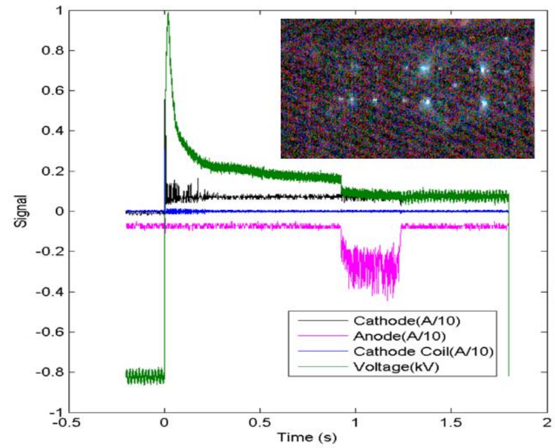

Figure 10. BOL Normal Gradient with Thruster Startup Event. *This plot shows the change in coupon substrate voltage (green) during a 400W Hall thruster startup, after exposure to normal gradient charging. Inset is first frame of high speed camera capture, showing glowing interconnects. Voltage change is initiated as thruster cathode turns on (black curve), and drops to zero after anode current (without magnets) is ignited in Hall thruster (magenta). Scope trigger occurs via AC-coupled current probe on cathode (blue).*

After normal gradient exposure, small but measurable changes were observed in the in-situ Dark IV and electroluminescence of the center string. As shown in Figure 9, a small hotspot appeared on the lower right edge of the top cell. Furthermore, there was a change of a few mA in the peak power region of the dark IV sweep of the center string, indicating a small reduction in shunt resistance.

C. BOL Normal Gradient with Thruster Startup

A total of 7 lab thruster startups were performed with the coupon pre-charged under normal gradient conditions. Based on early pathfinder testing with a different coupon, it was determined that a modest -1kV bias on the coupon was needed to properly observe the effect of thruster startup via the external circuit (otherwise all surface neutralization occurred via direct conduction to exposed conductors, bypassing the external circuit). This was not considered unreasonable as there is expected to be a nontrivial absolute structure potential during worst-case GEO charging conditions. If anything, this potential may be small.

The thruster startup from cathode ignition to full Hall discharge was performed manually and ideally occurred within a second. However, sometimes the full Hall discharge would not immediately ignite, and all the residual surface charge would be neutralized almost exclusively by the cathode (with a small portion neutralized by anode with no magnets). Initially, the current probe on the structure capacitor and the high voltage probe signals were used for the trigger, resulting in no recorded events. To force consistent triggering, the current signal from the cathode was used and the scope record lengths were increased to capture the entire startup.

Ultimately, it appeared that most of the activity occurred during the cathode-only portion of the startup. Negligible current was measured on the external current probes and no secondary discharge events were detected. However, as shown in Figure 10, there was a voltage swing from -1kV to +1kV over 20ms followed by a slow decay over a timescale of roughly a second towards zero. The initial process was likely due to cathode plasma ions slowly neutralizing the surface charge, resulting in a residual positive image charge on the substrate. Assuming a 1nF capacitance, this voltage jump would correspond to a 0.1mA flowing back to substrate common. Plasma electron repulsion ends shortly before the absolute surface potential reaches the floating potential. At this point, the substrate and string potentials would very slowly decay from +1kV by drawing electrons from the plasma into exposed conductors like interconnects. This indicates leakage currents under a microampere. The ions in the plasma clamp the absolute surface potential at the floating potential during this process.

The high speed camera captured another interesting aspect of this slow discharge. A faint blue glow was observed around the interconnects during the first ~10ms of the discharge (3 camera frames). This suggests that the local plasma environment may briefly allow some stored surface charge to conduct into exposed interconnects, neutralizing image charges. Note that the powered normal gradient test is a very conservative test in that solar cell current generation does not normally occur with normal gradient conditions (because they occur in eclipse) and therefore does not indicate an issue with the solar array design.

D. BOL Inverted Gradient with Thruster Startup

Only 3 thruster startups were attempted, two with structure capacitor current as trigger and one with cathode current as trigger. Full thruster startup only occurred on the cathode trigger event. Due to a configuration issue, the -1kV bias voltage was toggling incorrectly, resulting in spurious recharging of the substrate by the bias supply after cathode startup and spurious triggers. Nonetheless, similar to the normal gradient case, there were negligible currents measured on the external circuit. No discernable activity was observed on coupon by the high speed camera, throughout startup.

E. Lifetime XR-5 Plume Exposure

For the accelerated lifetime exposure, the coupon configuration in the chamber was altered so the coupon could be exposed continuously to the XR-5 plume. As shown in Figure 4, the coupon was placed 0.9m away from the XR-5, at 55° plume angle and 60° angle of incidence. The current density at 0.9m and 57° was expected to be ~0.4 A/m^2 for 400V, 7.5A operation of the XR5 [1]. Furthermore, the ion energy distribution at this angle was expected to include a significant fraction of ions with energy below the nominal anode voltage due to scattering and other processes [1,13,14]. Overall erosion of the coupon was predicted by convolving thruster plume data with total sputter yield (TSY) data [1,13-15]. The exposure at the 400V condition was predicted to remove all of the anti-reflective MgF_2 coating. Some minor exposures at 200V operating points provided additional margin.

Following the exposure, the coupon was removed and visually examined. The most striking change was a dramatic reduction in coverglass gloss. The ion fluence should have been sufficient to remove all the anti-reflective MgF_2 coating so presumably this was eroded glass. Contact surface resistivity measurements (with conductive rubber pads and a benchtop electrometer at 100V bias) were performed (in air) to determine whether any metal or carbon contamination occurred. The resistivity of both the pristine and the exposed coverglasses were at the TΩ limit, suggesting negligible conductivity and contamination. Dark IV performed before and after exposure at ambient conditions revealed no change in electrical performance. As will be discussed in Section J, the effect of this erosion on functional performance in light was surprisingly small, even when combined with degradation due to ESD. There were also mild shadow patterns produced behind raised wires and prayer tabs obstructing the ion beam, where surface erosion was reduced and sputter contamination was increased.

F. EOL Inverted Gradient

A total of 100 EOL inverted gradient events were recorded in the short span of 39 minutes. The arc rate significantly increased and the arcs moved exclusively to the interconnects rather than the substrate. As shown in Table 2, the current and charge flowing to or from the substrate dropped an order of magnitude. The string currents decreased slightly while charge increased, indicating broader discharges. As shown in Figure 11, the blue flashover glow is gone since there is no more MgF_2 coating. Instead, one can see the faint electroluminence of cells activated by transient currents. The uncoated glass is less prone to secondary electron production so only charges to 1.2kV.

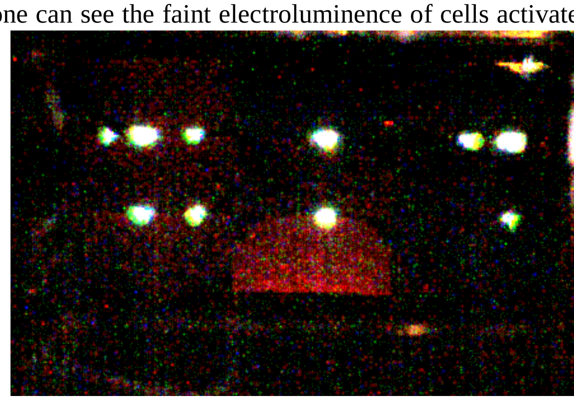

Figure 11. Composite Image of All EOL Inverted Gradient Events. *This image shows a per-pixel average of all high speed camera frames taken during end of life inverted gradient exposure.*

G. EOL Normal Gradient

The most dramatic change in discharge behavior before and after exposure occurred for normal gradient. As shown in Table 2, the maximum stored charge flowing from the substrate to the external circuit doubled to 126uC, resulting in a similar change in maximum return current into the strings terminals. The interval between arcs also doubled. More striking was the change in the spatial pattern of the discharge. Figure 12 shows a composite image of all EOL NG events. Streamers appear to follow nearly vertical lines on the coverglasses as well as a fainter diagonal striations emanating from the vertical edges of each cell. The vertical lines appear to follow the path of the incident ions, projected onto the surface.

The origin of this pattern formation is not clear but it is not without precedent. A number of studies have suggested ion erosion can produce periodic grooves and other patterns in surfaces under certain conditions [16-19]. If there is even the slightest pattern to the surface etching, streamers will tend to follow it.

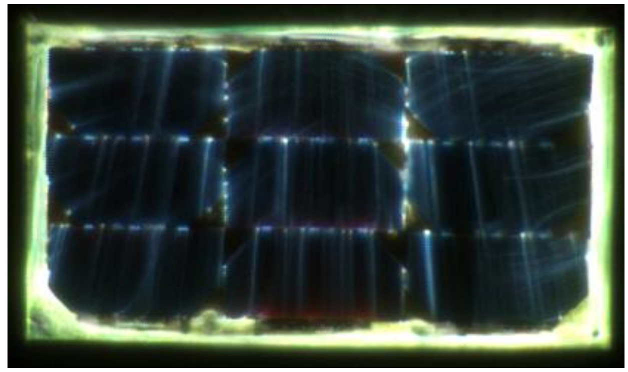

Figure 12. Composite Image of All EOL Normal Gradient Events. *This image shows a per-pixel average of all high speed camera frames taken during end of life normal gradient exposure.*

Similar to BOL, EOL NG also resulted in a couple temporarily sustained secondary discharge events. Figure 13 shows a typical event. In this case, ~0.25A flowed through the discharge for 25us. Like the BOL event, SAS2 was voltage limited, suggesting the resistance between string 2 and string 1 or substrate is 240 Ohms (including resistance along cells leading to the arc). From the high speed camera image, an arc along the edge between the top-center and top-right cells seems to be a likely secondary discharge location as this is where the differential potential between adjacent cells is greatest. However, there are also arcs between string 2 and substrate at the top of the left substring and bottom of the center substring that may contribute.

In situ dark IV curves and electroluminescence revealed small but measurable changes after this test. As shown in Figure 14, a new hotspot pair appeared on the lower right corner of the top-center cell and the upper-left corner of the middle-right cell. On String 1, there was a small reduction in shunt resistance, resulting in a ~10mA increase in dark current in the peak power region. Note that the powered normal gradient test is a very conservative test in that solar cell current generation does not normally occur with normal gradient conditions (because they occur in eclipse) and therefore does not indicate an issue with the solar array design.

H. EOL Normal Gradient with Thruster Startup

For EOL Normal Gradient, two different scope triggering schemes were used: cathode current trigger with -1kV bias and secondary interrupt (fast diode current) trigger. The former triggering scheme was used for 3 thruster startups, producing similar results to BOL. The latter triggering scheme was used for 12 more startups, detecting 5 secondary discharge events. The thruster startup routine was also significantly shortened relative to BOL tests by activating all the thruster power supplies before cathode ignition.

Since thruster ignition occurred nearly simultaneously with cathode ignition, the ambient plasma density and flux during surface neutralization was orders of magnitude larger than with cathode ignition alone. As a result, the substrate voltage jumped to its maximal value on a millisecond timescale (over an order of magnitude faster). The peak value was 0.4 to 1.1kV. The decay of the substrate potential was also orders of magnitude shorter, only 10 ms, due to the rapid collection of electrons through the exposed conductors. A typical startup transient is shown in Figure 15.

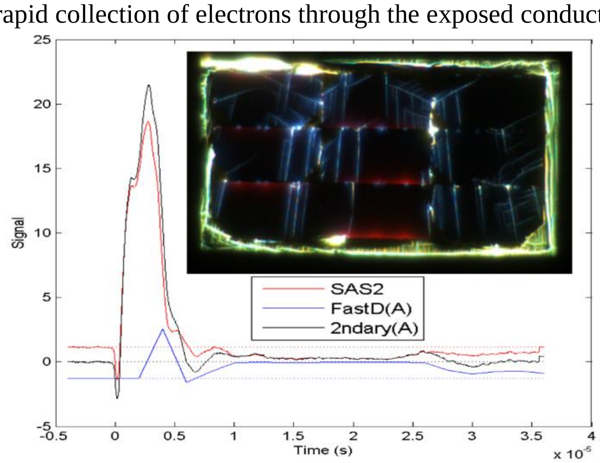

Figure 13. EOL Normal Gradient Event. *This plot shows current transients in Amperes from an individual ESD event. Inset is the associated high speed camera image of that event. See Figure 7b for curve identification.*

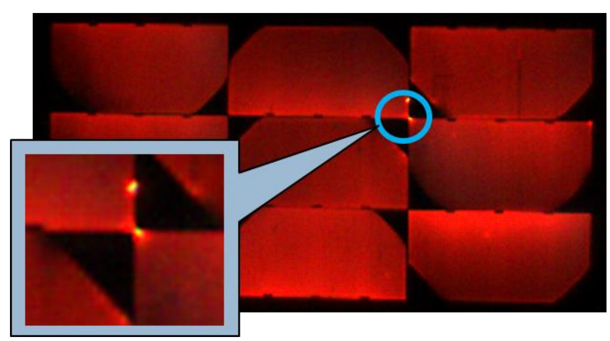

Figure 14. Electroluminescence after EOL Normal Gradient. *This image shows electroluminescence after EOL Normal Gradient exposure. A new hotspot feature is circled in light blue. Inset is exploded view of new hotspot at intersection of cells.*

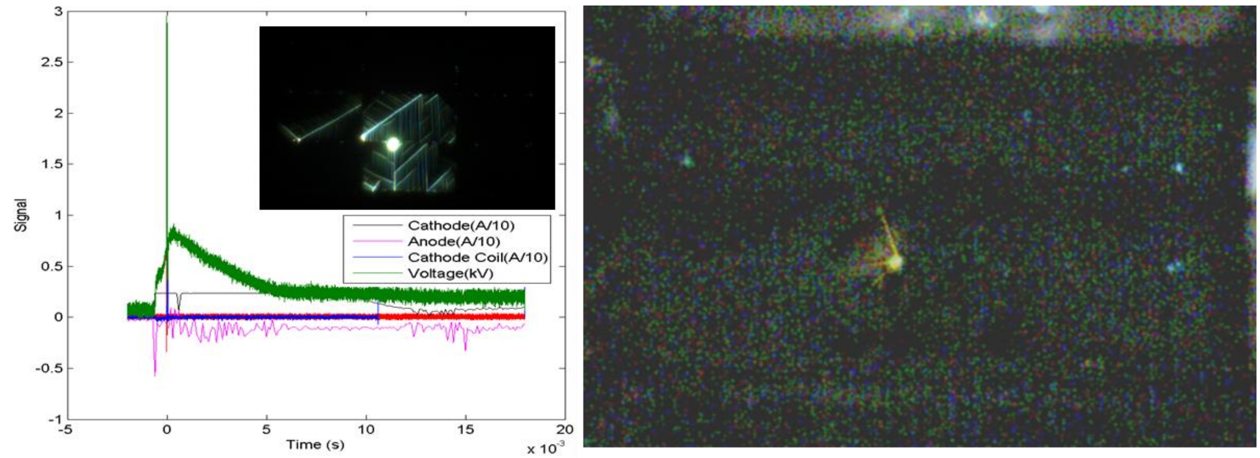

Figure 15. EOL Normal Gradient with Thruster Startup. *The plot on the left (a) shows the change in coupon substrate voltage (green) during a 400W Hall thruster startup, after exposure to normal gradient charging. Inset left is first frame of high speed camera capture, showing a large interconnect arc and streamers on the adjacent coverglasses. The image on the right (b) shows the second frame of the high speed camera (~3ms later) for the same event, showing glowing ejecta from the arc point.*

As consequence of this more rapid transition in surface and electrode potentials in a high density plasma is that more short-timescale transients were possible. The secondary current trigger was sensitive to both primary and secondary discharges. Brief 10µs voltage transients brought the substrate as high as 4kV before decaying down to the initial value before the transient. In these events, current on the order of an ampere oscillated back and forth between both terminals of both strings and the substrate for tens of microseconds. This in turn resulted in erratic spikes on the fast diode sensor, making it difficult to discern a clear secondary discharge signature outside of the primary event.

Although there may not have been any secondary discharges, there were primary discharges occurring during these startups. The inset of Figure 15a shows the first high speed camera frame of a typical ESD event: bright linear streamers crisscross coverglasses with arc points on the interconnects of cells. Figure 15b shows the subsequent frame for this event, which is atypical: the arc point between the middle and bottom-center cells continues to glow and appears to eject glowing material, indicating the arc point is getting particularly hot. The length of the streaks and the 3ms duration of each frame can be used to estimate a minimum velocity of 15m/s for the ejecta.

I. EOL Inverted Gradient with Thruster Startup

Similar triggering and fast thruster startup were used for the EOL IG tests. For simplicity, no bias was applied for either cathode or secondary interrupt trigger conditions. The two cathode triggers produced a change in high voltage down as low as -550V, coincident with startup, followed by a 20ms decay. This is consistent with electron neutralization of the surface followed by much slower ion conduction into the exposed conductors. All probe currents were negligible. No events occurred during the 10 startups using the secondary interrupt for trigger.

J. EOL Functional Tests

Ex-situ electroluminescence measurements performed and the beginning and end of the test campaign confirmed the presence of new hotspots on strings 1 and 2 from secondary discharge events. Electrical generation of the solar panel test coupon was measured using LAPSS to directly assess changes in operational performance. Due to the robust design of the solar panel the only measureable performance degradation expected was about a 2% to 3% drop in current due to the removal of the MgF_2 Anti-Reflective (AR) coating on the coverglass by the Xenon thruster plume. LAPSS illumination spectrum and intensity are calibrated to AM0 sunlight and are generally very repeatable (typically <<0.5%) so the expected 2-3% drop in current was well within the LAPSS measurement repeatability.

The measured normal-incidence LAPSS test results are shown in Table 3. The reduction in current and power due to both plume exposure and ESD events was only about 1%. This was significantly less than the 2-3% reduction expected due to the removal of the AR coating alone, which was predicted by erosion analysis and confirmed by inspection after the test. Dark IV measurements before and after ESD events further suggest that about half of the loss in I_{load} and P_{mp} was due to losses in cell performance following powered normal gradient test conditions.

Figure 16. Magnified BOL & EOL Coverglass Images. *Pristine AR Coated Coverglass (top) compared to a coverglass with the AR coating removed and textured by the EP plume (bottom).*

This is a very significant and unexpected result that may be explained by the very small scale surface texturing created by the Xenon ion plume erosion. Figure 16 shows a comparison at 1,000X magnification under a Keyence VHX-5000 microscope between the micro-scale texturing in the AR coated coverglass exposed to the EP plume and the smooth surface of the AR coated coverglass not exposed to the EP plume. It is hypothesized that the loss of the MgF_2 AR coating due to the EP plume (and corresponding loss in cell current) may be off-set by the AR properties of the fine-scale surface structure created by the EP plume. Surface structures with dimensions on the order of the wavelength of visible light (~0.5μm) have known anti-reflective properties [20]. If further research confirms this result then the power degradation due to EP plume exposure may be less than expected due to this phenomenon.

Satellite solar panels often receive off-normal illumination due to orbit inclination, orbital maneuvers, or seasonal variation of the sun angle relative to the earth. Thus, it is important to characterize the off-normal electrical generation of the solar panel coupon after EP plume exposure so that power can be predicted accurately. This was accomplished by LAPSS testing the coupon post exposure at angles ranging from +/- 85 degrees. The data from this testing is shown in Figure 17 and as expected shows that after EP plume exposure that current roll-off generally follows the cosine law, with a little additional roll-off at high angles, similar to a pristine solar panel prior to plume exposure.

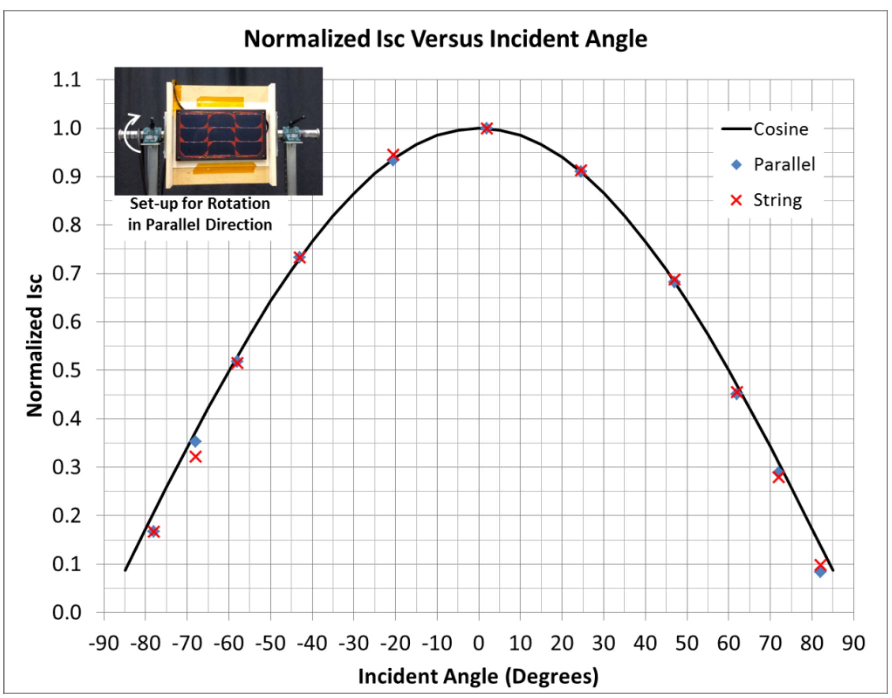

Figure 17. Test Panel Off-Normal Current Roll-Off After EP Plume Exposure Measured by the LAPSS.

Table 3. Change in Coupon Electrical Performance due to EP Plume Exposure Measured in Normal Incidence LAPSS Testing.

Parameter	Change Due to EP Exposure (Ave Circuit 1 & 2)	Expected Change
Isc	-0.5%	-2% to -3%
Iload	-1.0%	-2% to -3%
Pmax	-1.0%	-2% to -3%
Voc	0.1%	0%

IV. Conclusion

Overall this solar array coupon performed very well under the various EP and GEO-like plasma environments. The low bus voltage and current in the active circuit appears to have eliminated the risk of sustained secondary arcing in various ESD environments, consistent with the observations of Bodeau [21]. The few temporarily sustained secondary discharge events all occurred during powered normal gradient test, an unusually harsh condition that is not part of any testing standard. Indeed powered normal gradient on the front side of a solar array is very unlikely to occur, as large negative surface charges are rapidly eliminated by the same solar photons that would power the strings. A better way to view this test is as yet another way to generate the localized plasma necessary to initiate secondary discharges, similar to pulsed laser or particle impact-induced secondary discharge [10, 22]. This condition was clearly more harmful to the cells than inverted gradient as all changes in performance followed normal gradient exposures. Even so, the ultimate change in string performance was on the order of half a percent.

The EP plume erosion of the MgF_2 AR coating also had surprisingly little effect on the string performance. As noted above, P_{mp} only decreased by 1.0% after a simulated lifetime exposure (including the contribution from ESD). However, this erosion did have a significant effect on the character of the ESD events. The inverted gradient ESD was altered in part due to the removal of MgF_2, which can charge more positively because of its high secondary yield, and glows during flashover. However, additional changes after a lifetime exposure appeared to coerce all inverted gradient arcs to occur exclusively at the interconnects. More surprising was the change in visual appearance of the normal gradient arcs. Patterns etched in the coverglasses after lifetime exposure seem to guide discharge streamers in surprisingly linear paths. These patterns must be particularly subtle or shallow as they are not obvious even under 1000X magnification.

Acknowledgments

The authors would like to thank Jim Pollard, Kevin Diamant, and Simon Lui at the Aerospace Corporation and Kenneth H. Wright, Jr., Todd A. Schneider, and Jason A. Vaughn at NASA Marshall for useful discussions. We'd also like to recognize Nikki Noushkam for early development of the test plan and Joel Jermakian and Jim Wachholz for assistance in the final test circuit design. We'd like to thank John Nocerino from for performing in-house ex-situ functional tests on the solar array coupon and assisting in their interpretation. Finally, we wish to acknowledge the assistance of Phillip Mak, Mike Worshum, Byron Zeigler, and Kevin Dorman.

References

[1]Bermudez, L.M., Agathon-Burton, C.A., Basak, D., and Glogowski, M.J., "A Comprehensive Numerical Approach to the Modeling and Simulation of Plume Interaction Effects on Solar Electric Propulsion Spacecraft," IEPC Paper 2017-238, 35th International Electric Propulsion Conference, Atlanta, GA, October 2017

[2]Provost, S., Theroude, C., and Cheoux-Damas, P., "Overview of Astrium Erosion/Contamination Modelling Tool and Validation on ONERA Experimetal Results,'' IEPC Paper 2003-267, 28th International Electric Propulsion Conference, Toulouse, France, March 2003

[3]Hallock, G. A., Wiley, J. C., Khanna, A., and Spencer, E. A., "Impact Analysis of Hall Thrusters on Satellite Antenna Performance," Journal of Spacecraft and Rockets, Vol. 39, No. 1, Jan-Feb 2002, pp. 115-124.

[4]Likar, J.J., Bogorad, A.L., August, K.A., Lombardi, R.E., Kannenberg, K., and Herschitz, R., "Spacecraft Charging, Plume Interactions, and Space Radiation Design Considerations for All Electric GEO Satellite Missions," IEEE Transactions on Plasma Science, Vol. 43, Issue 9, September 2015

[5]Yalin, A., Topper, J., Farnell, C., Yoder, G., Hoang, B., and Corey, R., "Effect of Ion Sputtering on Transmission of Coverglass with Magnesium Flouride," IEPC Paper 2011-066, 32nd International Electric Propulsion Conference, Wiesbaden, Germany, Sept. 2011

[6]J. E. Pollard and K. D. Diamant, "Hall Thruster Plume Shield Wake Structure." AIAA 2003-5018, July 2003.

[7]Y. Raitses, L.A. Dorf, A.A. Litvak, and N.J. Fisch, "Plume reduction in segmented electrode Hall thruster," J. Appl. Phys., 88, April 2000, p. 1263.

[8]K. H. Wright et al "High Current ESD Test of Advanced Triple Junction Solar Array Coupon" IEEE Trans. Plasma Sci. Vol. 43, No. 9, Sept. 2015, pp. 2993-2999,

[9]T. Okamura et al., "Influence of Power Supplies on the Secondary Arc Test of Solar Arrays" J. Spacecraft & Rockets, Vol. 46, No. 3, June 2009, pp. 689-696.

[10]ISO-11221, "Space systems – Space solar panels – Spacecraft charging induced electrostatic discharge test methods," 2011.

[11]P. Leung, "Plasma phenomena associated with solar array discharges and their role in scaling coupon test results to a full panel," AIAA 2002-0628, Jan. 2002.

[12]A. E. Jensen & J. R. Dennison, "Defects Density of States Model of Cathodoluminescent Intensity and Spectra of Disordered SiO2." IEEE Trans. Plasma Sci., Vol. 43, No. 9, Sept. 2015.

[13]J. E. Pollard et al "Ion Flux, Energy, and Charge-State Measurements for the BPT-4000 Hall Thruster" AIAA 2001-3351, July 2001.

[14]L. M. Bermudez et al "High Fidelity Numerical Simulations for the Characterization of Plasma Plume Interaction Effects on Geostationary Satellites" AIAA 2015-4641, Sept. 2015

[15]Noushkam et al. "Sputtering Effects of Xenon Ion Thruster Plume on Common Spacecraft Materials" AIAA-2015-4642, Sept. 2015.

[16]P. Sigmund, "Theory of sputtering. I. Sputtering yield of amorphous and polycrystalline targets." Phys. Rev. 184 (2), 1969, p. 383

[17]P. Sigmund, "A mechanism of surface micro-roughening by ion bombardment." J. Mater. Sci. 8 (11), 1973, pp. 1545–1553.

[18]R. Mark Bradley, J.M.E. Harper, "Theory of ripple topography induced by ion bombardment." J. Vac. Sci. Technol. A: Vac. Surf. Films 6 (4), 1988, pp. 2390–2395.

[19]C.S.R. Matthes et al, "Fluence-dependent sputtering yield of micro-architectured materials." Applied Surface Science 407, 2017, p.223–235

[20]J. Son, et al, "Enhancement of optical transmission with random nanohole structures," Optics Express, A35, Vol. 19, No. S1, Jan. 2011.

[21]M. Bodeau, "Current and Voltage Thresholds for Sustained Arcs in Power Systems." IEEE Trans Plasma Sci., Vol. 40, No. 2, Feb 2012, pp. 192 - 200.

[22]L. Levy et al, "Simulation of In-flight ESD Anomalies Triggered by Photoemission, Micrometeoroid Impact and Pressure Pulse." IEEE Trans. Nucl. Sci., Vol. 44, No. 6, Dec. 1997, p. 2201-2208.